Draft version January 12, 2013
Preprint typeset using LaTeX style emulateapj v. 11/10/09

arXiv:1102.3664v1 [astro-ph.SR] 17 Feb 2011

ACCELERATION, MAGNETIC FLUCTUATIONS AND CROSS-FIELD TRANSPORT OF ENERGETIC ELECTRONS IN A SOLAR FLARE LOOP

E.P. Kontar, I.G. Hannah and N.H. Bian
School of Physics and Astronomy, University of Glasgow, G12 8QQ, UK

Draft version January 12, 2013

ABSTRACT

Plasma turbulence is thought to be associated with various physical processes involved in solar flares, including magnetic reconnection, particle acceleration and transport. Using Ramaty High Energy Solar Spectroscopic Imager (*RHESSI*) observations and the X-ray visibility analysis, we determine the spatial and spectral distributions of energetic electrons for a flare (GOES M3.7 class, April 14, 2002 23:55 UT), which was previously found to be consistent with a reconnection scenario. It is demonstrated that because of the high density plasma in the loop, electrons have to be continuously accelerated about the loop apex of length $\sim 2\times10^9$cm and width $\sim 7\times10^8$cm. Energy dependent transport of tens of keV electrons is observed to occur both along and across the guiding magnetic field of the loop. We show that the cross-field transport is consistent with the presence of magnetic turbulence in the loop, where electrons are accelerated, and estimate the magnitude of the field line diffusion coefficient for different phases of the flare. The energy density of magnetic fluctuations is calculated for given magnetic field correlation lengths and is larger than the energy density of the non-thermal electrons. The level of magnetic fluctuations peaks when the largest number of electrons is accelerated and is below detectability or absent at the decay phase. These hard X-ray observations provide the first observational evidence that magnetic turbulence governs the evolution of energetic electrons in a dense flaring loop and is suggestive of their turbulent acceleration.

Subject headings: Sun:flares - Sun: X-rays, gamma rays - Sun:activity - Sun:particle emission

1. INTRODUCTION

In the standard flare scenario, the magnetic energy stored in the solar corona is released accelerating particles. However, despite decades of effort, the exact mechanisms remain elusive. It is still unclear how and where exactly the particles are energized. Hard X-ray (HXR) imaging spacecrafts such as Yohkoh/HXT (Kosugi et al. 1991) and RHESSI (Lin et al. 2002) are particularly useful for the spatial and spectral diagnostics of energetic particles (Shibata 1999; Aschwanden 2002; Lin et al. 2003; Brown & Kontar 2005; Lin 2006; Temmer et al. 2010). Masuda et al. (1994, 1995); Sui et al. (2004); Liu et al. (2008); Joshi et al. (2009) have reported observations of a non-thermal HXR source above the top of an X-ray loop, suggesting coronal energy release via magnetic reconnection (see Priest & Forbes 2002, as a review).

Along with magnetic reconnection, another important element of the standard flare model is magnetohydrodynamic (MHD) turbulence as it is believed to play a key role in a number of processes, from triggering fast reconnection to particle acceleration and transport. A considerable number of particle acceleration theories have been developed that require the presence of magnetic fluctuations in the flaring loop. Assuming a high level of MHD waves, it has been shown that stochastic acceleration can effectively accelerate a large number of both electrons and ions (Miller & Ramaty 1987; Hamilton & Petrosian 1992; Melrose 1994; Miller et al. 1997; Petrosian & Bykov 2008; Bykov & Fleishman 2009; Bian et al. 2010; Petrosian & Chen 2010). These particle acceleration models include both resonant and non-resonant interaction between the particles and various plasma waves. Waves and turbulence can be associated either with current sheets during magnetic reconnection (Chiueh & Zweibel 1987; Somov & Kosugi 1997; Litvinenko 2006) or with reconnection outflows (Larosa et al. 1994). As the magnetic field in the solar corona is weak compared to the photosphere, direct measurement of even the mean field in the corona is problematic. Therefore, the fluctuating components of the coronal magnetic fields and their relation to energetic particles remain unknown. In addition, the location and physics of turbulent acceleration within the general picture of magnetic energy release is still awaiting an observational basis.

In this paper, using RHESSI X-ray observations and the visibility analysis technique, we show, for the first time, the presence of energy dependent cross-field transport of energetic electrons in a flaring loop. We estimate the relative magnitude and energy density of magnetic fluctuations which is required to explain these observations. We show that these HXR observations provide a quantitative basis for the turbulence measurements and its governing role in the evolution of energetic electrons and are suggestive of turbulent electron acceleration in this loop.

2. LIGHTCURVES, SPECTRA, AND SPATIAL DISTRIBUTION OF X-RAYS FROM A FLARING MAGNETIC LOOP

We select a GOES M3.7 class flare, well-observed by RHESSI, which was previously analyzed by Sui et al. (2004); Veronig & Brown (2004); Bone et al. (2007); Xu et al. (2008). Sui et al. (2004) reported the existence of an X-ray source moving above the X-ray loop and concluded that the observations were consistent with the pic-

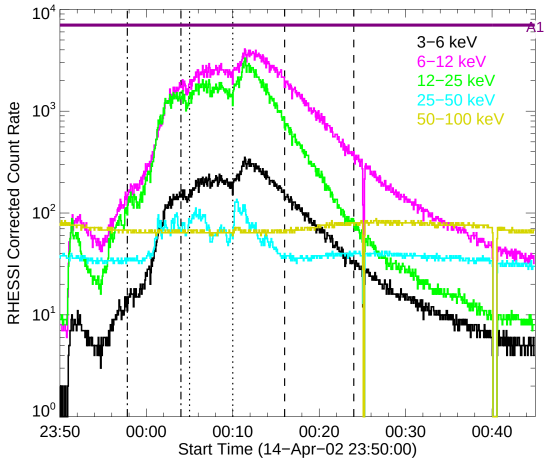

FIG. 1.— Time profile in different RHESSI energy ranges of the 2002-04-14 event starting near 23:55 UT. The vertical lines indicates the three time periods for which the spectra, images and visibility forward fitting were performed.

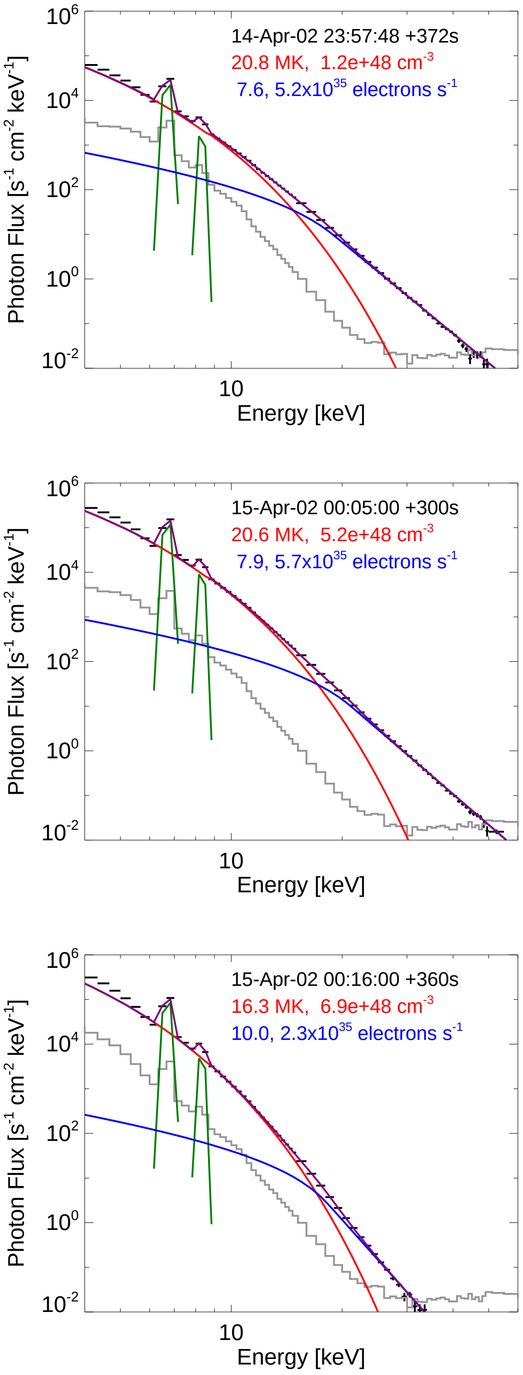

FIG. 2.— The spatially integrated RHESSI X-ray spectra (black data points) for the three time intervals during the flare. These spectra were obtained using all front detectors excluding 2 and 7 (see Smith et al. 2002, for details) fitted (purple line) with an isothermal (red line) plus thick-target nonthermal (blue line) model. The pre-flare background spectra are shown in grey.

ture of the formation and development of a current sheet between the loop-top and coronal source. This April 14, 2002 $23:55$ UT flare (Figures 1-3) shows a simple loop structure over the whole duration of the flare and, importantly, the magnetic loop is filled with dense plasma $n \sim 10^{11}\mathrm{cm}^{-3}$ (Veronig & Brown 2004). Unlike the majority of solar flares, which typically produce the soft X-ray (SXR) emission in the coronal part of the loop and bright HXR emission in the dense chromospheric footpoints (e.g. Emslie et al. 2003; Kontar et al. 2008), the source of HXRs is coronal for this flare. Because of the high plasma density in the loop (Table 1), energetic electrons of $10-20$ keV are collisionally stopped in the coronal part of the loop and produce thick-target emission (Brown 1971). At the same time, for such a dense loop, 20 keV particles have collisional lifetime $\lesssim 0.1$s, so electrons need to be continuously accelerated in order to explain the observed HXR emission.

We analyse this flare in three time intervals corresponding to the rise, peak and decay phases (see Fig 1). From the X-ray spectra (Fig 2), we determine the electron acceleration rate dN/dt and the inverse power-law spectral index δ of non-thermal electrons, assuming a collisional thick-target model (Brown 1971). We also obtain from an isothermal component in the spectral fit (Holman 2005): the electron temperature T_e and the emission measure of thermal plasma, i.e. $EM = n^2V$, where n is the plasma density and V is the volume occupied by the thermal plasma.

During the initial phase of the flare, acceleration of electrons up to ~ 50 keV is observed along with rapid heating of the plasma up to a temperature of 20 MK (Fig 2). As the flare progresses, the thermal plasma emission measure grows while the temperature slightly increases reaching 23 MK. The acceleration rate dN/dt is found to be around $\sim 5\times10^{35}$ electrons s^{-1}. In the decay phase of the flare, the thermal plasma starts to cool, the spectrum of energetic electrons steepens and the number of non-thermal electrons drops. The main flare parameters are summarized in Table 1.

X-ray images reconstructed using the CLEAN algorithm (Hurford et al. 2002) for the three time intervals are presented in Figure 3. A clear loop structure is observed up to $\sim$ 20 keV. Since RHESSI measures the spatial distribution of X-rays only indirectly, via rotating modulating collimators (Hurford et al. 2002), X-ray images can suffer from their reconstruction artifacts (Prato et al. 2009; Battaglia et al. 2011) and should not

TABLE 1
HXR magnetic loop and flare parameters for the event starting April 14, 2002 23:55UT.

Time	L(10keV) (10^8cm)	W(10keV) (10^8cm)	EM (10^{48}cm^{-3})	T_e (MK)	V ($\pi W^2 L/4$) (10^{26}cm^3)	$n = \sqrt{EM/V}$ (10^{10}cm^{-3})	δ	dN/dt (10^{35} elec s^{-1})	$\mathbf{B}_\perp^2 \lambda_\parallel / \mathbf{B}_0^2$ (10^7cm)
23:57:48-00:04:00	20.3	4.8	1.2	21	1.4	9.3	7.3	5.2	2.3
00:05:00-00:10:00	22.0	7.5	5.2	20	3.7	11.8	7.8	5.7	2.3
00:16:00-00:24:00	23.5	11.2	6.9	16	8.9	8.8	9.8	2.3	$\lesssim$0.8

be used to determine the spatial size of the source. Instead, a more direct and hence reliable approach is to 'stack' the rotationally-modulated lightcurves over a number of spacecraft spin periods to produce X-ray visibilities (Hurford et al. 2002; Schmahl et al. 2007). The latter are instrument-independent 2-dimensional Fourier components of the HXR source (Schmahl et al. 2007). For a simple source geometry, as displayed in this flare, the position and sizes can be determined unambiguously at various energies. An additional advantage of the X-ray visibility fitting approach is that the statistical errors can easily be propagated to find the uncertainties associated with the inferred parameters of the loop (Kontar et al. 2008; Prato et al. 2009). Kontar et al. (2008, 2010) have successfully proved the robustness and sub-arcsecond precision of this method for HXR footpoints. X-ray visibilities are fitted using a curved elliptical gaussian model of the flare (Hannah et al. 2008; Xu et al. 2008). This is done for a number of energy ranges between 9-20 keV and for the three time intervals (see Fig. 3). The Full Width Half Maximum (FWHM) source sizes, specifically the length $L(\epsilon)$, and width $W(\epsilon)$ and their corresponding statistical uncertainties, are obtained and presented in Figure 4. Using L and W at energy 10 keV, we find the volume $V = \pi W^2 L/4$ occupied by the thermal plasma. Assuming a volume filling factor of unity, the plasma density is calculated: $n = \sqrt{EM/V}$ (Table 1). It is found to be similar to the previous density estimates (Veronig & Brown 2004; Bone et al. 2007; Xu et al. 2008).

As anticipated from the thick-target scenario in a weakly changing plasma density (see Brown et al. 2002, for details), the source length, $L(\epsilon)$, in the direction parallel to the guiding magnetic field, is a growing function of energy. The reason is that higher energy electrons can propagate further away from the region were they are accelerated, hence making the HXR source larger along the guiding field. In other words, in a dense coronal source, electrons travel a distance determined by their collisional losses. The stopping distance of an electron emitting X-rays of energy ϵ while moving along the guiding field of the loop is $r_\parallel \simeq \epsilon^2/(2Kn)$, where $K = 2\pi e^4 \ln\Lambda$, e is the electron charge, $\ln\Lambda \simeq 20$ is Coulomb logarithm (Brown et al. 2002). For an energy independent length L_0 of the acceleration region, the FWHM length of the source is given by (Xu et al. 2008):

$$L(\epsilon) = L_0 + \alpha_\parallel \epsilon^2. \tag{1}$$

By fitting Equation (1) to the measured $L(\epsilon)$, it is possible to determine L_0 and $\alpha_\parallel$ [arcsec keV^{-2}]. Figure 4 shows that the length of the acceleration region L_0 is around $\sim 2\times10^9$ cm at the peak of the flare. Moreover, since $n = (2K\alpha_\parallel)^{-1}$, $\alpha_\parallel$ can be used as an independent measure to determine the plasma density. This approach gives plasma densities of 9.8×10^{10}cm^{-3}, 2.9×10^{11} cm^{-3}, 1.7×10^{11}cm^{-3} for the three time intervals analyzed in this paper. These densities are within a factor of two from the ones which were inferred above by using the thermal emission of the flare (see Table 1). Larger densities at the peak and decay phases of the flare can be attributed to the presence of a colder plasma invisible in Soft X-rays (SXR) with RHESSI, as suggested in previous studies of thermal sources (e.g. Jakimiec et al. 1998).

3. ENERGY-DEPENDENT WIDTHS OF THE LOOP

The CLEAN images (Figs. 3) show that the loop width (size perpendicular to the guiding field) is like the length, growing with energy. This is seen quantitatively with the visibility forward fitted as a function of energy in Figure 4. A growing width $W(\epsilon)$ with energy is clearly present in the first and second time intervals (Figure 4) but could be absent in the third. This is particularly surprising as the guiding magnetic field is strong enough to ensure pure field-aligned transport of energetic electrons. Indeed, for a mean magnetic field of ~ 150 Gauss as measured in this loop using radio data (Bone et al. 2007), the Larmor radius of tens of keV electrons is ~ 2 cm and, therefore, the trajectories of their guiding centers coincide with the magnetic field lines. Collisions are unimportant in producing perpendicular transport for the parameters of the plasma, only resulting in a radial excursion (classical collisional diffusion) of the order of the electron gyroradius in a collisional time.

However, it is well-known that particle transport across a mean magnetic field can be dramatically enhanced, well above the collisional value, in the presence of turbulence. The reason is the braiding of the field lines themselves due to perpendicular magnetic fluctuations. In the presence of magnetic fluctuations $\mathbf{B}_\perp$ perpendicular to the mean field ($\mathbf{B}_0 = B_0\mathbf{z}$), perpendicular transport of field lines occurs which is governed by the following equation: $d\mathbf{r}_\perp(z)/dz = \mathbf{B}_\perp(\mathbf{r}_\perp(z), z)/B_0$ (Rechester & Rosenbluth 1978). Field lines braiding is believed to be a dominant process governing the transport of particles in the solar wind (Jokipii 1966), in laboratory plasmas (Bickerton 1997), and in thermal coronal loops (Galloway et al. 2006). It is safe to neglect the contribution of perpendicular electric fluctuations and subsequent $\mathbf{E}\times\mathbf{B}$ drift to cross-field transport. For MHD fluctuations, the electric field is $E_\perp \sim v_A B_\perp/c$ such that the magnetic drift $\mathbf{v}_B = v_\parallel(\mathbf{B}_\perp/B_0)$ dominates over the electric drift $\mathbf{v}_E = c\mathbf{E}_\perp \times \mathbf{B}_0/B_0^2$ (c is the speed of light and v_A is the Alfven velocity). Since $v_B/v_E \sim v_\parallel/v_A$, the contribution of the $\mathbf{E}\times\mathbf{B}$ drift to perpendicular transport is negligible for non-thermal electrons with energies above $\gtrsim 10$ keV ($v_\parallel \simeq 6\times10^9$ cm s^{-1}), i.e. $v_\parallel \gg v_A$, with $v_A \simeq 10^8$ cm s^{-1} in the magnetic loop. The magnetic field

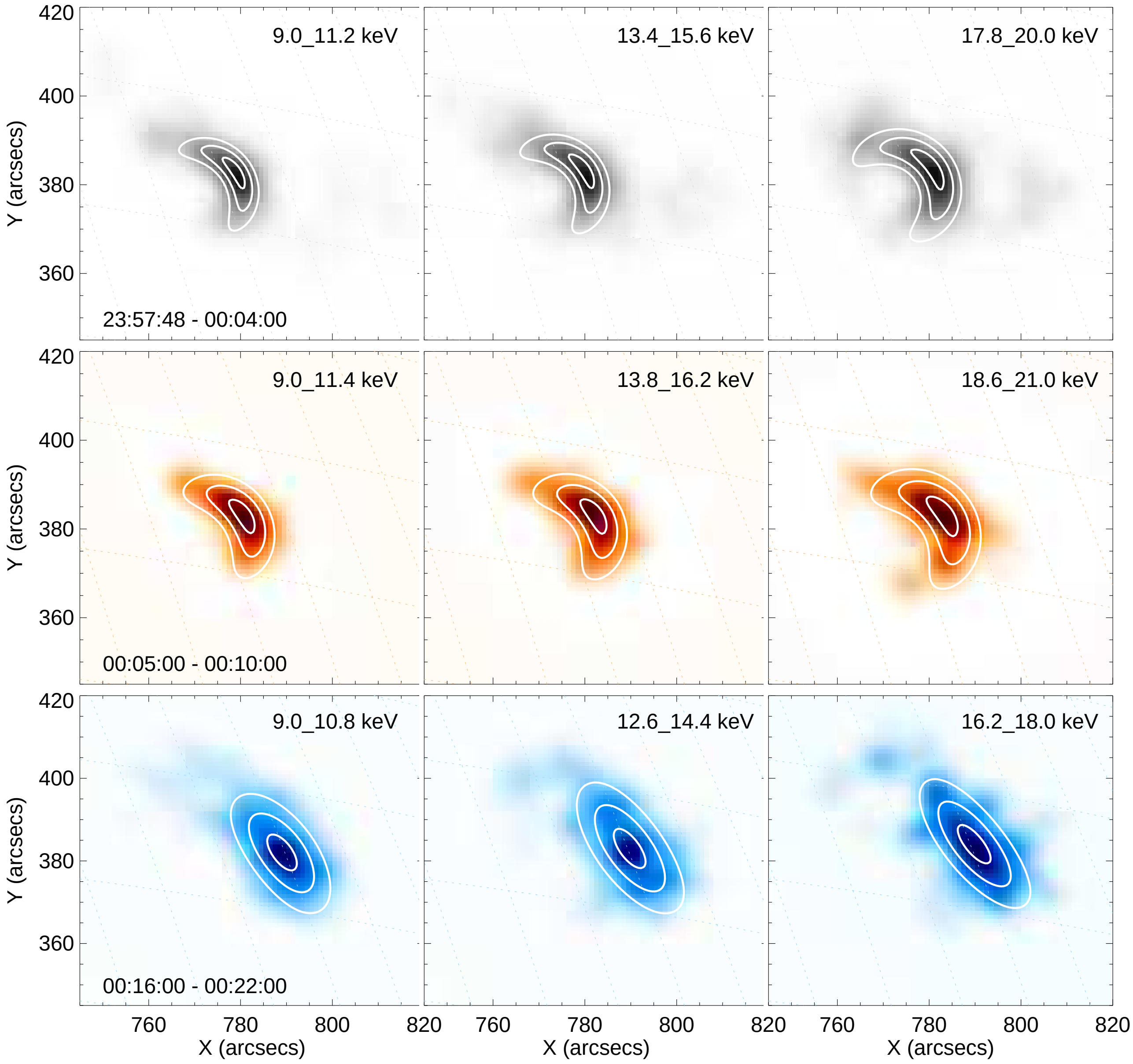

Fig. 3.— CLEAN image overlayed by 30, 60 and 90% levels from the forward fitting to X-ray visibilities. Each row indicates a different time range. Each column a different energy range. The parameters of the loop are summarized in Table 1 and Figure 4.

line diffusion coefficient is given by the Taylor formula: $D_M = (1/B_0^2)\int_0^\infty d\zeta < \mathbf{B}_\perp(\mathbf{r}_\perp(\zeta),\zeta)\mathbf{B}_\perp(\mathbf{r}_\perp(0),0) >$. Here, $< \mathbf{B}_\perp(\mathbf{r}_\perp,z)\mathbf{B}_\perp(0,0) >$ is the two-points correlation function and $<>$ denotes an ensemble average. In the quasi-linear approximation, the perpendicular transport of field lines is characterized by a diffusion coefficient $D_M \simeq (B_\perp^2/B_0^2)\lambda_\parallel$, where $\lambda_\parallel$ is the parallel correlation length of the perturbations $\mathbf{B}_\perp$ (Jokipii & Parker 1969; Rechester & Rosenbluth 1978). An electron moves a distance $r_\parallel \simeq \epsilon^2/2Kn$ along the mean field in a collisional life-time. Therefore, this electron also makes a radial excursion given by $r_\perp = \sqrt{2D_M r_\parallel}$, as a consequence of the radial transport of field lines. This means that the FWHM width of the source $W(\epsilon)$ should also grow with energy. It is the sum of the acceleration region width W_0 and the diffusion part due to perpendicular transport:

$$W(\epsilon) = W_0 + \alpha_\perp \epsilon, \tag{2}$$

where $\alpha_\perp = \sqrt{2D_M\alpha_\parallel}$ is measured in arcsec keV^{-1}. The unique feature of this expression is that it depends on the level of magnetic fluctuations via the magnetic field line diffusion coefficient D_M. Therefore, by measuring the energy dependent width of the flaring magnetic loop (Figure 4), we find automatically the diffusion coefficient for the magnetic field lines, i.e. $D_M = \lambda_\parallel B_\perp^2/B_0^2 = \alpha_\perp^2/(2\alpha_\parallel)$ (Table 1). As anticipated, $W(\epsilon)$ can be well

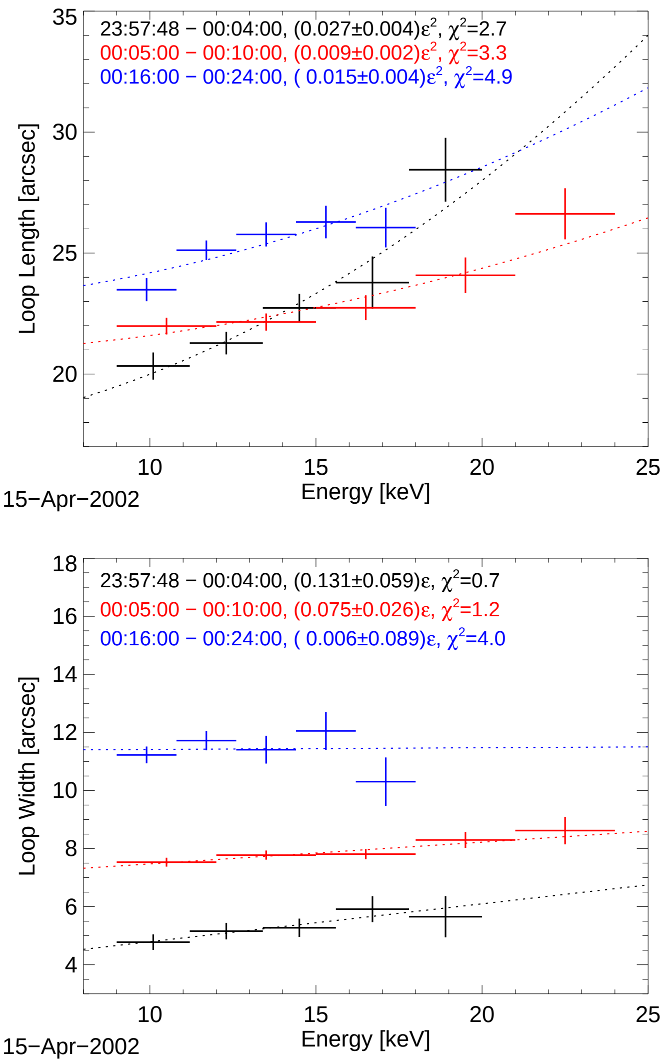

FIG. 4.— The FWHM loop lengths (top) and widths (bottom) found from forward fitting the loop shape to the visibilities. The fitted lines are of the form $L(\epsilon) = L_0 + \alpha_{\|}\epsilon^2$ and $W(\epsilon) = W_0 + \alpha_{\perp}\epsilon$ for the lengths and widths respectively. The full χ^2 quoted are calculated using the statistical uncertainties from X-ray visibility fits. $\alpha_{\perp}$ and $\alpha_{\|}$ are measured in units of [arcsec keV^{-1}] and [arcsec keV^{-2}] respectively.

fitted with a linear fit (Figure 4) to find $\alpha_{\perp}$ and the magnitude of magnetic fluctuations. The magnetic diffusion coefficient $\lambda_{\|}B_{\perp}^2/B_0^2$ is changing with time and is strongest when the acceleration rate dN/dt of non-thermal electrons is at the maximum and the spectral index of the accelerated electrons is smaller (hardest HXR spectrum). The magnitude of fluctuations at the decay phase is weaker, so the data cannot provide a reliable estimate, but only an upper limit.

The energy density of magnetic fluctuations in the loop is $B_{\perp}^2/8\pi \simeq (B_0^2/8\pi)D_M/\lambda_{\|}$. Taking the length of the acceleration region 2×10^9 cm as the upper limit for correlation length $\lambda_{\|}$, the energy density of magnetic fluctuations is $\simeq 10$ erg cm^{-3} and the relative level of fluctuations $B_{\perp}/B_0 \sim 0.1$. For $\lambda_{\|} = 2.3\times 10^7$ cm, the magnetic perturbations follow to be strong $B_{\perp}/B_0 = 1$, and the energy density of turbulence $\simeq 900$ erg cm^{-3}. This value is close to the energy density of the flaring plasma $3nk_BT_e \simeq 830$ erg cm^{-3} and much larger than the energy density of the non-thermal electrons

$$U_{nth} = \frac{1}{S}\int_{E_c}^{\infty} E\frac{F(E)}{\sqrt{2E/m_e}}\mathrm{d}E, \tag{3}$$

where $S = \pi W_0^2/4$ is the cross-sectional area of the loop, $F(E > E_c) \propto E^{-\delta}$ is the thick-target acceleration rate differential in energy [electrons s^{-1} keV $^{-1}$], and E and m_e are the electron energy and mass respectively. Using the values from thick-target fit and loop width measurements, the energy density of non-thermal electrons, U_{nth} is about 11, 6, and 1 erg cm^{-3} for the three time intervals respectively. Therefore, we can conclude that the energy density of the magnetic turbulence is sufficient to energize at least non-thermal electrons and possibly the whole flare.

4. DISCUSSION AND CONCLUSIONS

X-ray visibility based analysis has allowed us to infer the energy dependent source size for a well observed flaring loop. Both the length and the width of the loop are found to be larger at higher energies. This is in clear contrast with HXR footpoints, which show the opposite trend; higher energy sources appear smaller than lower energy sources (Kontar et al. 2008; Prato et al. 2009; Kontar et al. 2010). An energy dependent growth of the loop length is expected from the collisional precipitation of energetic electrons along field lines (Brown et al. 2002; Xu et al. 2008). The high density of the loop implies that the electrons are accelerated inside the loop region with the characteristic size 2×10^9 cm. At the same time, the size of the loop perpendicular to the strong magnetic field is an increasing function of energy. The increase of the loop width implies strong cross-field transport of non-thermal electrons and is found to be consistent with the diffusion of magnetic field lines. This allows us to determine the level and locations of magnetic fluctuations in the flaring loop. For comparison, we note that the magnetic diffusion coefficient $D_M = \lambda_{\|}B_{\perp}^2/B_0^2$ measured *in situ* in the solar wind, where $B_{\perp}/B_0 \sim 1$ and $\lambda_{\|} \sim 10^{11}$ cm (Matthaeus et al. 1986) is about four orders of magnitude larger than our values presented in Table 1.

We note that although the length and width of the flare are likely to be governed by parallel transport and diffusion of the magnetic field lines, equations (1,2) for the width and the length are approximations. The simultaneous treatment of acceleration, energy losses and cross-field transport is needed to assess the particle dynamics more accurately. This might lead to super or sub-diffusive cross-field transport of electrons and cannot be ruled out by the current data, so the radial excursions can scale as $r_{\perp} \propto \epsilon^{\beta}$, with β close to one. Nevertheless, the width-energy measurements provide a powerful and unique tool to measure magnetic fluctuations in a flaring plasma. Importantly, the energy density of magnetic fluctuations appears to be energetically significant and is found to be larger than the energy density of non-thermal particles.

The temporal and spatial analysis by Sui et al. (2004) of the weaker source above the dense loop analyzed here suggests a picture consistent with formation of a reconnecting current sheet between the loop top and the coronal source. Assuming this reconnection scenario, our observations suggest the presence of MHD turbulence in the loop under the reconnection site. During the event, the length of acceleration site increases only by $\sim 10\%$, while the width of the bright HXR loop W_0 grows with time more than a factor of ~ 2, which could be attributed to continuous piling up of newly reconnected lines. The plasma mode responsible for the perturbations remain unknown, but these observations indicate the presence of noticeable magnetic fluctuations during the solar flare inside the loop, where the acceleration of electrons is happening. It is possible to speculate that the magnetic field fluctuations are produced by magnetic reconnection above the loop and accelerate electrons inside the flaring loop.

This work is partially supported by a STFC rolling grant. Financial support by the Leverhulme Trust (EPK), and by the European Commission through the SOLAIRE (MTRN-CT-2006-035484) and HESPE (FP7-SPACE-2010-263086) Networks is gratefully acknowledged. The overall effort has greatly benefited from support by a grant from the International Space Science Institute (ISSI) in Bern, Switzerland.

REFERENCES

Aschwanden, M. J. 2002, Space Sci. Rev., 101, 1
Battaglia, M., Kontar, E. P., & Hannah, I. G. 2011, A&A, 526, A3+
Bian, N. H., Kontar, E. P., & Brown, J. C. 2010, A&A, 519, A114+
Bickerton, R. J. 1997, Plasma Physics and Controlled Fusion, 39, 339
Bone, L., Brown, J. C., Fletcher, L., Veronig, A., & White, S. 2007, A&A, 466, 339
Brown, J. C. 1971, Sol. Phys., 18, 489
Brown, J. C., Aschwanden, M. J., & Kontar, E. P. 2002, Sol. Phys., 210, 373
Brown, J. C., & Kontar, E. P. 2005, Advances in Space Research, 35, 1675
Bykov, A. M., & Fleishman, G. D. 2009, ApJ, 692, L45
Chiueh, T., & Zweibel, E. G. 1987, ApJ, 317, 900
Emslie, A. G., Kontar, E. P., Krucker, S., & Lin, R. P. 2003, ApJ, 595, L107
Galloway, R. K., Helander, P., & MacKinnon, A. L. 2006, ApJ, 646, 615
Hamilton, R. J., & Petrosian, V. 1992, ApJ, 398, 350
Hannah, I. G., Christe, S., Krucker, S., Hurford, G. J., Hudson, H. S., & Lin, R. P. 2008, ApJ, 677, 704
Holman, G. D. 2005, Advances in Space Research, 35, 1669
Hurford, G. J., Schmahl, E. J., Schwartz, R. A., et al. 2002, Sol. Phys., 210, 61
Jakimiec, J., Tomczak, M., Falewicz, R., Phillips, K. J. H., & Fludra, A. 1998, A&A, 334, 1112
Jokipii, J. R. 1966, ApJ, 146, 480
Jokipii, J. R., & Parker, E. N. 1969, ApJ, 155, 777
Joshi, B., Veronig, A., Cho, K., Bong, S., Somov, B. V., Moon, Y., Lee, J., Manoharan, P. K., & Kim, Y. 2009, ApJ, 706, 1438
Kontar, E. P., Hannah, I. G., Jeffrey, N. L. S., & Battaglia, M. 2010, ApJ, 717, 250
Kontar, E. P., Hannah, I. G., & MacKinnon, A. L. 2008, A&A, 489, L57
Kosugi, T., Masuda, S., Makishima, K., Inda, M., Murakami, T., Dotani, T., Ogawara, Y., Sakao, T., Kai, K., & Nakajima, H. 1991, Sol. Phys., 136, 17
Larosa, T. N., Moore, R. L., & Shore, S. N. 1994, ApJ, 425, 856
Lin, R. P. 2006, Space Sci. Rev., 124, 233
Lin, R. P., Dennis, B. R., Hurford, G. J., et al. 2002, Sol. Phys., 210, 3
Lin, R. P., et al. 2003, Advances in Space Research, 32, 1001
Litvinenko, Y. E. 2006, A&A, 452, 1069
Liu, W., Petrosian, V., Dennis, B. R., & Jiang, Y. W. 2008, ApJ, 676, 704
Masuda, S., Kosugi, T., Hara, H., Sakao, T., Shibata, K., & Tsuneta, S. 1995, PASJ, 47, 677
Masuda, S., Kosugi, T., Hara, H., Tsuneta, S., & Ogawara, Y. 1994, Nature, 371, 495
Matthaeus, W. H., Goldstein, M. L., & King, J. H. 1986, J. Geophys. Res., 91, 59
Melrose, D. B. 1994, ApJS, 90, 623
Miller, J. A., Cargill, P. J., Emslie, A. G., Holman, G. D., Dennis, B. R., LaRosa, T. N., Winglee, R. M., Benka, S. G., & Tsuneta, S. 1997, J. Geophys. Res., 102, 14631
Miller, J. A., & Ramaty, R. 1987, Sol. Phys., 113, 195
Petrosian, V., & Bykov, A. M. 2008, Space Sci. Rev., 134, 207
Petrosian, V., & Chen, Q. 2010, ApJ, 712, L131
Prato, M., Emslie, A. G., Kontar, E. P., Massone, A. M., & Piana, M. 2009, ApJ, 706, 917
Priest, E. R., & Forbes, T. G. 2002, A&A Rev., 10, 313
Rechester, A. B., & Rosenbluth, M. N. 1978, Physical Review Letters, 40, 38
Schmahl, E. J., Pernak, R. L., Hurford, G. J., Lee, J., & Bong, S. 2007, Sol. Phys., 240, 241
Shibata, K. 1999, Ap&SS, 264, 129
Smith, D. M., Lin, R. P., Turin, P., et al. 2002, Sol. Phys., 210, 33
Somov, B. V., & Kosugi, T. 1997, ApJ, 485, 859
Sui, L., Holman, G. D., & Dennis, B. R. 2004, ApJ, 612, 546
Temmer, M., Veronig, A. M., Kontar, E. P., Krucker, S., & Vršnak, B. 2010, ApJ, 712, 1410
Veronig, A. M., & Brown, J. C. 2004, ApJ, 603, L117
Xu, Y., Emslie, A. G., & Hurford, G. J. 2008, ApJ, 673, 576